Quantitative 3D X-ray imaging of densification, delamination and fracture in a micro-composite under compression

Bø Fløystad, Jostein; Skjønsfjell, Eirik Torbjørn Bakken; Guizar-Sicairos, Manuel; Høydalsvik, Kristin; He, Jianying; Andreasen, Jens Wenzel; Zhang, Zhiliang; Breiby, Dag Werner

Published in:
Advanced Engineering Materials

Link to article, DOI:
10.1002/adem.201400443

Publication date:
2015

Document Version
Peer reviewed version

DOI: 10.1002/ ((please add manuscript number))
Article type: Full Paper

Title: Quantitative 3D X-ray Imaging of Densification, Delamination and Fracture in a Micro-Composite under Compression

*Jostein Bø Fløystad, Eirik Torbjørn Bakken Skjønsfjell, Manuel Guizar-Sicairos, Kristin Høydalsvik, Jianying He, Jens Wenzel Andreasen, Zhiliang Zhang, Dag Werner Breiby**

Dr. J. B. Fløystad, Mr. E. T. B. Skjønsfjell, Dr. K. Høydalsvik, Prof. D. W. Breiby
Department of Physics
Norwegian University of Science and Technology
Høgskoleringen 5
N-7491 Trondheim, Norway

Dr. M. Guizar-Sicairos
Paul Scherrer Institut
CH-5232 Villigen PSI, Switzerland

Prof. J. He, Prof. Z. Zhang
Department of Structural Engineering
Norwegian University of Science and Technology
Høgskoleringen 5
N-7491 Trondheim, Norway

Dr. J. W. Andreasen
Department of Energy Conversion and Storage
Technical University of Denmark
Frederiksborgvej 399
DK-4000 Roskilde
Denmark

Keywords: X-ray ptychography; fracture mechanics; composites; tomography

(Abstract):

Phase-contrast three-dimensional tomograms showing in unprecedented detail the mechanical response of a micro-composite subjected to a mechanical compression test are reported. The X-ray ptychography images reveal the deformation and fracture processes of a 10 μm diameter composite, consisting of a spherical polymer bead coated with a nominally 210 nm metal shell. The beginning delamination of the shell from the core can be directly observed

already at an engineering strain of a few percent. Pre-existing defects are shown to dictate the deformation behavior of both core and shell. The strain state of the increasingly compressed polymer core is assessed quantitatively through the local densification at sub-micron resolution, supported by finite element analysis. Nanoscale mechanics is of rapidly growing importance in materials science, biotechnology and medicine, and this study demonstrates the use of coherent X-ray microscopy as a powerful tool for *in situ* studies of the mechanical properties of nanostructured devices, structures and composites.

1. Introduction

Being able to reliably measure mechanical response at the nanoscale is an important challenge for the continued development of bio- and nanotechnology. Micro electro-mechanical systems (MEMS) involve sensors and actuators, and optimal performance requires a well understood and carefully calibrated mechanical reaction to external stimuli.[1] Structural objects like spacers, electrical connects and micro-electronics packaging also need well-defined mechanical properties, partially owing to challenges with different thermal expansion coefficients.[1c] The mechanics of microscale composite structures is frequently modeled using finite element analysis (FEA),[1c] often with only indirect experimental verification owing to the scarcity of techniques able to measure mechanical response on sub-micron length scales.

Contact mechanics was established with Hertz' analytical small-strain solution for the elastic deformation- and stress fields associated with solids in frictionless contact.[2] Analytical contact mechanics is currently undergoing a revival[3] owing to its importance in bio-, nano- and microtechnology. A classical experiment of contact mechanics is that of a sphere exposed to a flat-punch compression test, which has been carried out at length scales ranging from meters to micrometers over the years.[4] Note that in many nanoindentation experiments, only

force versus displacement data are measured, leaving ample room for speculation about the actual deformation mechanism.

The strain state is of particular importance for the physical behavior of nanostructures.[5] Although the complications with strain add to the challenges of producing useful nanoscale devices, there are also several well-known examples where the extra degrees of freedom provided by manipulation of strain have been exploited for achieving desired device characteristics, perhaps most notably in bandgap engineering[5c] and increased charge carrier mobility.[6] Measuring the displacement of inherent or fiducial surface markers was the first method used to indirectly observe local strain fields.[7] This approach has been applied using a variety of imaging techniques including the Moiré fringe projection method, video microscopy,[8] electron microscopy,[9] and atomic force microscopy,[10] in the latter case achieving a spatial resolution of the strain field down to 500 nm. A common limitation of these methods is that they only observe the two-dimensional strain field near a surface, and in materials lacking features that can be tracked, markers need to be introduced, possibly altering the response of the material. Methods for tracking fiducial markers using X-ray computed tomography (CT) or magnetic resonance imaging (MRI)[11] have been developed to measure the complete strain tensor in three dimensions.[12] Diffraction-based methods can map strain in three dimensions on a per-crystallite basis in polycrystalline materials,[13] with recent developments in X-ray scattering techniques beginning to address strain mapping of amorphous materials in two dimensions.[14] It has recently been demonstrated that techniques based on coherent diffractive X-ray imaging can image the displacement field inside perturbed crystals.[15]

Beyond the elastic regime the device or composite changes irreversibly, often reported as deviations from Hookian behavior or “yield”, eventually leading to destruction. Fracture

mechanics, describing the formation and propagation of cracks, includes *delamination*, which is a key degradation mechanism of composites.[16] Measuring delamination nondestructively at the micro- and nanoscale is challenging, and the possible influence of (partial) delamination on stress-strain curves is of concern for reliable data interpretation. Standard CT is well suited for investigating macro- and microscale fracture, including delamination, with best reported spatial resolutions of just under 1 micrometer.[17] Improved techniques for monitoring delamination towards the nanoscale are thus in high demand.

The *densification* of a solid material, here defined as the density increase of a solid material in response to compressive stress, is a crucial parameter for describing the material state. For some polymers, particularly glassy thermoplastics, hydrostatic pressure tends to cause local yielding known as crazing,[18] resulting in a network of fine cracks. In addition to crazing, which is clearly an irreversible process, also elastic densification is a common phenomenon in polymers, as evidenced by the very existence of sound waves. In the literature, CT has recently been used to monitor the human vertebral collapse with associated densification – however with a resolution in the mm range.[19] There is clearly ample motivation for exploring the promise held by recently developed new phase-contrast X-ray microscopy methods like ptychography for significantly augmenting the toolbox for nano-mechanical studies.

In the present work, we apply *in situ* ptychographic tomography based on coherent X-ray scattering to monitor mechanical compression testing of a micron-sized polymer-metal composite. We follow the deformation, densification and fracture of a silver-coated polymer bead with 10 micrometer diameter at increasing compressive displacement during a classical flat punch experiment. From the quantitative 3D tomography data we obtain the local material densification at sub-micron resolution, which we compare to FEA calculations. We identify

structural weaknesses suggesting how these functional composites can be improved to sustain higher strain levels, which is important for the many foreseen applications, for example as anisotropic conducting adhesives in microsystem engineering.[20]

2. Ptychography

X-ray ptychography,[21] a scanning-based realization of the wider family of coherent diffractive imaging (CDI) techniques, has over the last few years emerged as a non-destructive microscopy approach with resolution currently down to about 16 nanometer in 3D.[22] The core idea of ptychography is to obtain real-space images of the object by applying phase retrieval algorithms[23] to measured far-field scattering patterns obtained with coherent radiation, as illustrated in **Figure 1**. Thus, instead of using an objective lens to form the image, the image is formed through computation. Owing to the weakly refracting nature of X-rays, it is technically difficult to make high quality objective lenses. Being able to evade the use of lenses is thus considered an important step for progress in X-ray microscopy.[21] The data required to reconstruct a ptychography image is a set of several (tens to thousands) far-field scattering patterns, all obtained with the same coherent, micron-sized X-ray beam at different spots on the object, together covering the field of view. Maintaining a high degree of overlap between the regions probed by separate neighboring exposures introduces redundancy in the measured data that makes ptychographic reconstruction robust. When combined with CT techniques, ptychography provides a direct *quantitative* measurement of the local electron density $\rho_e(\mathbf{r})$ in three dimensions.[24] Phase contrast images obtained with ptychography have excellent sensitivity also to light elements, ensuring applicability also for cells and biomaterials.[24a, 25] Finally, ptychographic imaging can be used to cover large fields of view, and the penetrating nature of X-rays allows both thick (tens of microns) samples and complex

sample environments. For all these reasons, *in situ* ptychographic tomography is starting to find applications in materials science.[25b, 26]

3. Ptychography Setup for in situ Mechanical Testing

The investigated composite microparticle consisted of a moderately crosslinked (2-5 %) acrylate methacrylate copolymer polymer core coated with a nominally 210 nm thick silver shell. A custom sample holder compatible with the tomography measurements, illustrated in **Figure 2**, was designed for the *in situ* mechanical compression experiments. A single composite microparticle was placed on the flat polished tip of a brass pin, measuring approximately 50 μm × 50 μm. Above the sample, a similar, parallel brass surface was held in place by an arm connecting it to the rest of the sample holder. A linear stick-slip piezoelectric actuator was used to control the separation between the two brass surfaces, allowing the bead to be compressed in steps Δd down to 50 nm; steps of 100 to 400 nm were employed. We define the normalized displacement (engineering strain) as $\eta = 1 - d / d_0$, where d is the separation between the brass surfaces (see Figure 1b) and d_0 is the initial diameter of the composite. The brass plates contacting the sample were slightly non-parallel, in effect obscuring the contact regions between the sample and brass plates from view. An offset of 1.7 μm caused by shadowing of the contact points thus had to be taken into account when calculating η, which ranged from $\eta = 0$ to $\eta = 0.29$ over the course of the experiment. The described sample holder was mounted atop piezoelectric actuators controlling the position of the sample holder in three dimensions, similar to the setup described by Dierolf *et al.*[24a] An air-bearing rotation stage was used to set the tomographic projection angle ω about a vertical axis through the sample, as indicated in Figure 1.

The compression experiment was performed quasi-statically under *displacement* control and without measurement of the applied load: η was increased in steps by decreasing the separation between the surfaces contacting the sample. Comparison with separate nanoindentation measurements[20] (not shown) indicates that the applied load reached approximately 8 mN at maximum. Time-dependent stress relaxation effects are unlikely to be relevant to our experiment as the relevant time constants in these polymers are known to be in the order of seconds. Starting approximately one minute after each compression step, we acquired a tomogram while the separation d between the top and bottom surfaces was kept constant.

A strained body will generally change its density compared to the unstrained state. This effect can be measured by the densification e, related to the normal true strain components ε_{ii} and density ρ by

$$e = -\left(\varepsilon_{xx} + \varepsilon_{yy} + \varepsilon_{zz}\right) = \frac{\rho - \rho_0}{\rho_0} \tag{1}$$

to first order in ε_{ii}, where the density of the unstrained body is ρ_0. This relation holds both for mass density and electron density $\rho_e(\mathbf{r})$, the latter of which is measured by ptychographic tomography. Consequently, the local densification $e(\mathbf{r})$ can be obtained with the high resolution provided by the tomography measurement.

4. Results and Discussion

An example of a reconstructed pair of absorption and phase-contrast projection images is shown in **Figure 3**. The projection images resolve the inhomogeneous metal shell and the polymer core of the composite, as well as the surrounding air. The counterintuitive flatness of the projection image originates from the fact that the optical path length is essentially constant

owing to the high density of the thin metal coating; a single component solid sphere would exhibit a phase shift decaying to zero at the perimeter.

Segmented CT reconstructions of the same bead at different η are presented in **Figure 4**, starting from zero displacement. We estimated the resolution of the tomograms to be better than 200 nm, as judged by the finest resolved details. Additionally, Fourier shell correlation[27] suggested 160 nm. The apparent thickness of the metal shell in the tomograms varied from below 200 nm to approximately 700 nm in different locations. In addition to experimental uncertainty, this apparent thickness is to be interpreted as a convolution of the actual inhomogeneous thickness with the experimental resolution. The electron density of the polymer was measured to be $\rho_0 = 0.38 \pm 0.02$ Å^{-3} for the unstrained bead, corresponding to a reasonable mass density of 1.15 ± 0.05 g cm^{-3}.

Initially, the metallic shell covered the entire polymer core with the exception of a few comparably small holes of diameters up to 500 nm. Some of these minor holes must be ascribed to numerical fluctuations and segmentation instabilities, while others were seen to be the initiation points of fractures, see below. At least one of the holes in the shell was also accompanied by a similarly shaped depression in the surface of the polymer sphere at the same location.

As η was increased, we observed deformation of the composite in the form of an increased horizontal diameter concomitant with the vertical compression. Theoretically, while the polymer close to the contact points must experience plastic deformation already at small η (< 0.05) because of the high local stress, elastic deformation is expected to dominate in the remainder of the composite up to moderate (~ 0.1) normalized displacement η.[4] From

comparing the exact shape of the compressed bead in the elastic regime to models, one may in principle determine elastic constants, notably the Poisson's ratio, but in the current experiment, the resolution proved insufficient for this kind of analysis.

The first observation of irrefutably irreversible response to the applied compression was the delamination of the silver shell from the polymer, as shown in Figure 4. Cohesive fracture formation in both the shell and the core followed at approximately the same η ~0.12. The cracks in the polymer core ran mainly parallel to the compression axis, extending radially inwards from the surface of the bead. Notably, an early crack formed at the mentioned depression in the surface of the polymer core (cf. lower right of all subfigures in Figure 4). In a similar fashion, the first major cracks in the shell connected pre-existing holes in the silver coating, as can be discerned on the left side of Figure 4c) and d). The progression of the deformation and fracture illustrates that the weakest part of the composite was the bonding between the polymer core and the metal shell.

The densification $e(\mathbf{r})$ is shown for several different η in **Figure 5**. The density of the polymer does not exhibit exact rotational symmetry, and especially not when approaching fracture. However, rotationally averaging the signal to reduce statistical variations gives a reasonable estimate of the polymer response, as supported also by the approximate horizontal mirror symmetry of the measured densification, see Figure 5. The densification remained localized to regions close to the contact points with the sample holder for small and moderate η, with the rest of the polymer core being largely unaffected. Upon approaching the critical displacement $\eta_c = 0.11 \pm 0.02$ required to fracture the bead, we observed increased densities throughout most of the polymer. Close to the axis of compression, the densification reached $e = 0.18$. At the first signs of fracture the densification decreased, presumably as a consequence

of the stress being partially relieved by the cracks, giving a spatial distribution of the densification reminiscent of a small-displacement ($\eta < 0.02$) state.

From the local true strain calculated using FEA, we obtained the densification as described by Equation (1); Figure 5 shows the densification obtained from such calculations. The magnitude and spatial distribution of the densification agree well between the simulated and experimental data. The processed data of Figure 5 shows local fluctuations in the densification which is understood to be partially noise. Still, by the significant correlation between the patterns obtained for different η, we speculate that some of these variations might arise from grains and other inhomogeneities. Because the finite element model assumes a homogeneous material, such inhomogeneities would not be correctly predicted. To further emphasize and summarize the findings of the present work, **Figure 6** presents tomographic cross sections taken perpendicular to the compression axis. Note in particular the changing density distribution with increasing η, the delamination and the fracture formation.

5. Perspectives

The continued efforts currently being done at synchrotrons for further improving the ptychography setups will lead to both significantly faster data collection and improved resolution. For extending the study described here, incorporating a miniature strain gauge for simultaneous stress measurements would be an obvious improvement. Also, using tools like focused ion beams (FIB), improved sample preparation would allow the contact areas to be studied.

As a highly relevant suggestion for the future use of the method for densification measurements described here, we would like to mention biomaterials.[28] In biotechnology,

efforts towards experimentally assessing the mechanical properties of cells, bacteria, viruses and tissue represent a modern and exciting research area.[28] The importance of understanding the mechanical properties of biomaterials is emphasized by the interest in creating synthetic materials mimicking their high-performance structures.[29] These materials frequently exhibit a complex, hierarchical morphology at several length scales which has a defining impact on their properties. The hierarchical structures allow them to sustain remarkably strong stress- and strain fields,[5a, 5b] but how their complex structure contributes to these properties is not well understood. Studies of bone and nacre [5a, 5b] have revealed that although these light-weight materials are formed from brittle and soft components, the resulting composites have remarkable strength. Direct and model-independent measurement of the local deformation, densification and beginning fracture formation in such materials under mechanical load would be important for understanding their mechanical properties.

Finally, again referring to bio-related specimens, we foresee that the emerging role of ptychographic microscopy as a tool for studying living organisms in solution[30] in the near future can be combined with biomechanical testing through adequate microfluidic sample environments.

6. Conclusion

In conclusion we have used ptychographic tomography to study a micro-composite *in situ* during compression, following deformation, local densification, and fracture formation eventually leading to the structural collapse of the composite. Weaknesses already existing in the as-synthesized composite, such as holes in the coating and depressions in the polymer surface, were demonstrated to influence the location of emerging cracks. Exploiting the quantitative nature of ptychographic tomography, we were able to compare the measured local densification inside the composite with predictions from finite element modelling,

finding good agreement; this opens for retrieving a whole range of previously inaccessible information from nanostructured materials and devices. Our findings show that studies of the densification as obtained from ptychographic tomography can be used to directly draw conclusions on the strain distributions of materials and to validate simulations of mechanical experiments. Through this work we have demonstrated the potential of ptychographic tomography for studying the mechanics of multi-component systems on sub-micron length scales.

7. Experimental Details

A. Composite Sample:

The polymer core of the core-shell microcomposite was a moderately crosslinked (2-5 %) acrylate methacrylate copolymer without additives, forming a sphere with diameter 10 μm supplied by Mosaic Solutions AS (Dragonveien 54, N-2013 Skjetten, Norway) as "Spherica 10". This bead was electrolessly coated with silver to form a shell nominally 210 nm thick.

B. Ptychographic Tomography:

Ptychographic tomography experiments were performed at the X12SA ("cSAXS") beamline at the Swiss Light Source, Paul Scherrer Institut, Villigen, Switzerland. A double Si(111) crystal monochromator defined the X-ray energy to 6.200 keV while an uncoated SiO_2 mirror suppressed higher harmonics. Approximately 5 mm upstream of the sample position, a 2 μm diameter pinhole was installed to define the lateral extension of the X-ray beam, also ensuring near perfect transverse coherence. The described sample holder was mounted atop piezoelectric actuators controlling the position of the sample holder in three dimensions, similar to the setup described by Dierolf *et al.*[24a] An air-bearing rotation stage was used to set the tomographic projection angle ω about a vertical axis through the sample, as indicated

in Figure 1. The setup allowed acquiring tomographic projections from an angular range of 177°, as the arm connecting the upper and lower parts of the sample holder blocked the X-ray beam for a range of 3°. A Pilatus 2M area detector[31] with square pixels measuring 172 μm was used to collect the scattering patterns 7.201 m downstream from the sample position.

The tomograms were acquired with projections spaced 1°, 2° or 4° apart in ω while the separation *d* between the top and bottom surfaces was kept constant. The temperature was 24 °C throughout the experiments. Each projection covered a field of view of approximately 18 μm × 16 μm and required 136 scattering patterns placed with ~1.3 μm between neighboring exposures to be measured, each with an exposure time of 0.10 s. The total time (including motor movements) for acquiring a tomogram was from 40 to 150 minutes, depending primarily on the chosen number of projections. This procedure was repeated with the sample being compressed in steps of 100 - 400 nm well beyond fracture formation, i.e. until the composite had disintegrated into several parts.

Over the course of the experiment, consisting of fifteen tomograms, the polymer core was subjected to a total radiation dose of 4 ± 1 MGy, with average and peak dose rates of approximately 50 Gy s^{-1} and 4 kGy s^{-1}, respectively. This dose is smaller than previous reports of similar tomographic imaging studies.[25a] The primary forms of beam damage in polymers are scission (the cutting of a polymer chain) and crosslinking (the formation of new bonds between chains). Considering the dose applied, it is probable that such changes at the molecular scale occur to some extent. In a previous test experiment using a Fresnel zone plate rather than a pinhole, thus giving two orders of magnitude higher photon flux, the polymer was observed to “vaporize” out of the metallic coating and to redeposit on the outer side of the coating. In the experiment reported here, we did not observe any indications of beam

damage, and while it cannot be ruled out that changes in the chemical structure affect the elastic moduli of the material, our results are fully consistent with an undamaged polymer.

Phase projection images were obtained from the measured far-field scattering patterns using the difference map[21b] and maximum likelihood [32]reconstruction algorithms based on the scattering signal up to a momentum transfer of $7.2 \cdot 10^{-3}$ Å^{-1}. To obtain the tomograms from phase projections, the projections were pre-processed as described elsewhere,[33] and the "simultaneous algebraic reconstruction technique" (SART) algorithm was used for the CT reconstruction, also enforcing non-negative electron densities.[34]

C. Numerical Reconstructions:

Using a 192 × 192 pixel square detector region for the ptychographic reconstructions yielded a reconstructed image pixel size of 43.6 nm. The resolution of this experiment was limited by a number of factors, predominantly: the mechanical stability of the position of the sample with respect to the probe, the number of tomography projections, the stability of the phase-field of the incoming X-ray beam (the "probe"), and the inherent contrast of the sample itself. The obtained resolution, estimated to 160 - 200 nm, thus allowed shorter wavelength oscillations in the numerical reconstructions, as seen in Fig. 3.

The three-dimensional electron density maps obtained from the tomographic reconstruction were expected to have only small changes in density between neighboring voxels within each material category (polymer bead, metal coating, surrounding air). This insight and the above resolution considerations suggest that excessive fluctuations can be reliably averaged and/or filtered out, as was done for Figs. 4-6. The de-noising technique "total variation minimalization",[35] was applied to the reconstructed tomograms for segmentation (Fig. 4).

The de-noised tomograms had well-preserved edges and sufficient contrast to allow segmentation.

D. Finite Element Analysis:

Finite element analysis was performed using the commercial software Abaqus (version 6.11-1, Dassault Systemes, 10 Rue Marcel Dassault, 78140 Vélizy-Villacoublay, France) as described in our previous articles on these micro-composites,[36] carefully including corrections for non-linear effects at large deformations. Exploiting symmetry around the compression axis and the mirror symmetry around the plane halfway between the contact planes, we modeled an octant of the sphere using about 400 four-node axisymmetric elements. The brass surfaces in contact with the sphere were treated as rigid surfaces, and frictionless contact was assumed. Young's modulus and Poisson's ratio of the polymer were taken to be 1 GPa and 0.3, respectively. The metal coating was ignored for these calculations.

Supporting Information

A movie illustrating the tomography experiment is available as Supporting Information from the Wiley Online Library or from the corresponding author.

Acknowledgements

We thank Helge Kristiansen of Conpart AS for supplying the composites and Ole Tore Buset, Tor Arne Vassdal and Julio Cesar Da Silva for technical assistance. The Norwegian Research Council is gratefully acknowledged for financial support.

Received: ((will be filled in by the editorial staff))
Revised: ((will be filled in by the editorial staff))
Published online: ((will be filled in by the editorial staff))

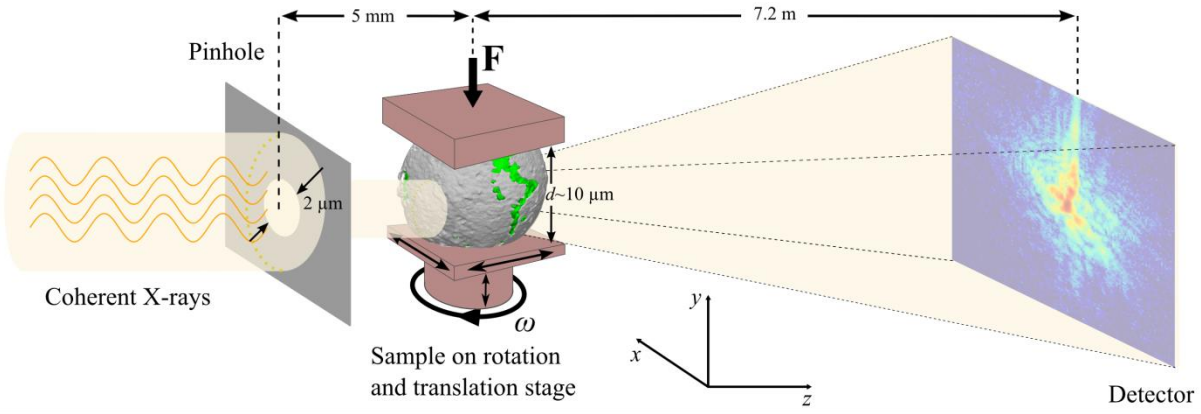

Figure 1. Experimental ptychographic set up. Coherent X-rays are incident on a 2 µm diameter pin hole before propagating to the sample 5 mm downstream. The microcomposite is placed in a parallel-plate sample holder that can compress and maintain a constant spacing *d*. Translation and rotation stages make it possible to raster scan the sample in the *xy*-plane for different projection angles ω. The X-rays scattered by the sample will propagate 7.2 m further downstream to the detector where one scattering pattern is recorded for each sample position.

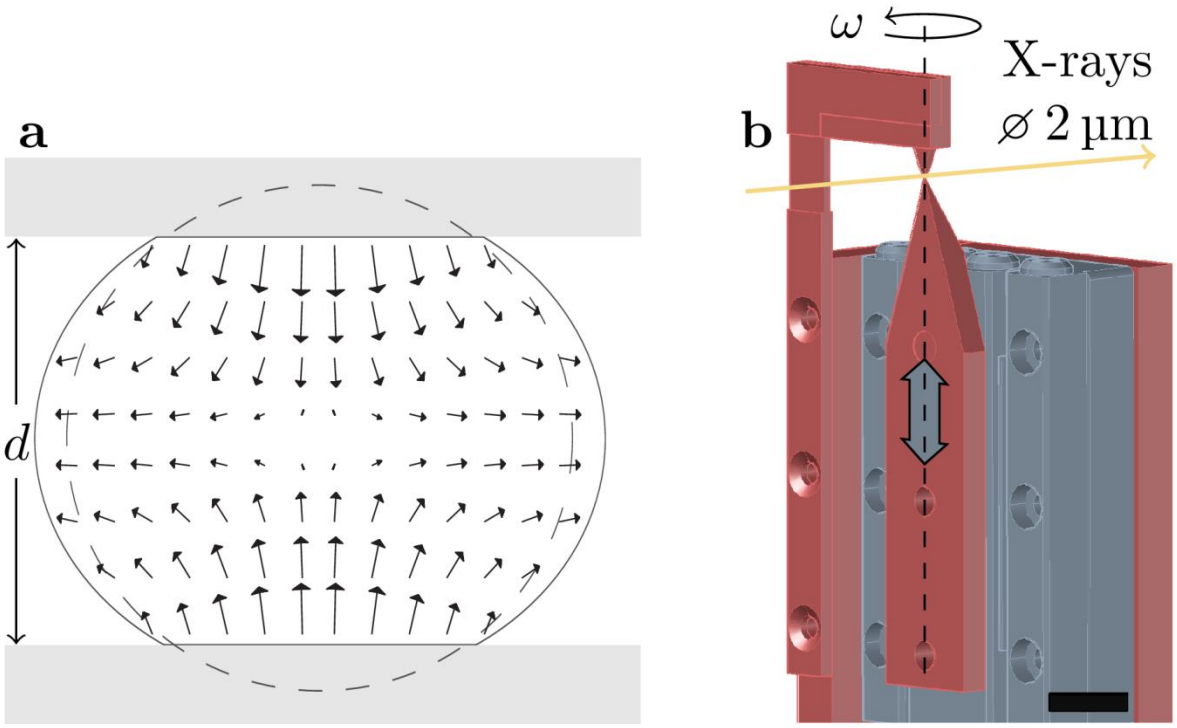

Figure 2. a) Illustration of how the pristine sphere (dashed lines) is expected to deform under an axial compressive load, with the displacement field indicated by arrows. *d* denotes the separation between the surfaces contacting the sample. b) Sketch of the sample cell used for compressing specimens during ptychographic tomography experiments. The sample was mounted between the two highly pointed, yet locally flat and nearly parallel brass surfaces and positioned in the narrow X-ray beam (yellow arrow). A linear actuator indicated in gray color controlled the separation *d* between the brass plates (Scalebar 5 mm)

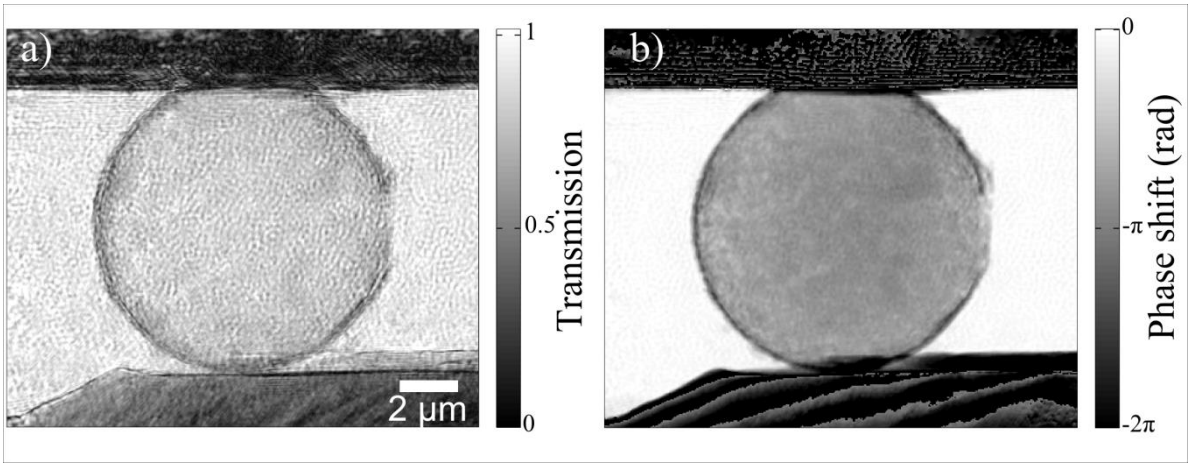

Figure 3. Example pair of ptychographic projection images, a) absorption contrast, b) phase contrast. The small features seen in particular in the absorption image are numerical artefacts, consistent with the fact that whereas the reconstructed pixel size is 43.6 nm, the spatial resolution obtained is closer to 200 nm.

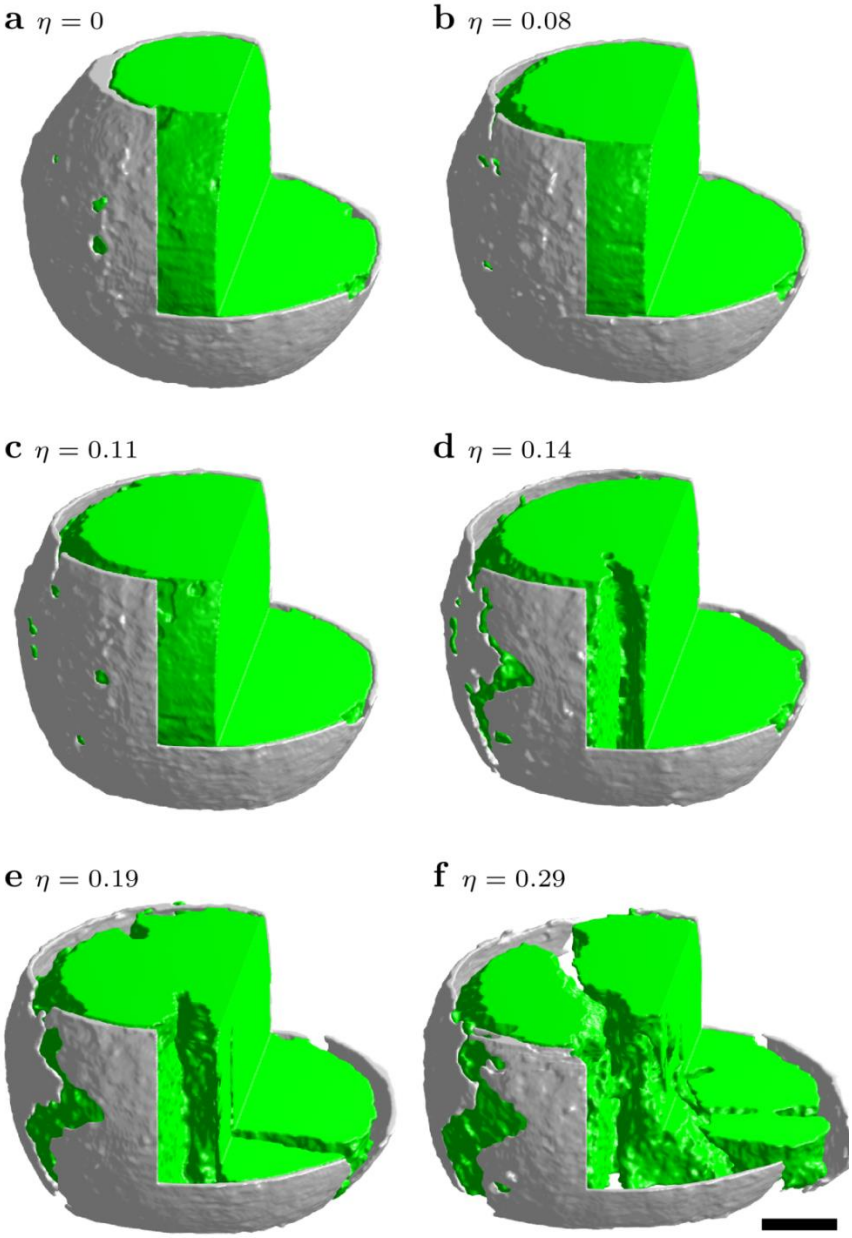

Figure 4. Cutaway view of 3D renderings of the polymer core (green) and silver coating (grey) for selected increasing η. a) The initial state of the bead before compression. The metal shell covers the entire polymer with the exception of a few small holes with diameters up to 500 nm. b) The applied compression has caused the metal shell to start detaching from the polymer core at some locations. c-f) Further compression has led to essentially full delamination of the shell and caused cracks to form in both the metal coating and the polymer core. Scalebar 2 μm.

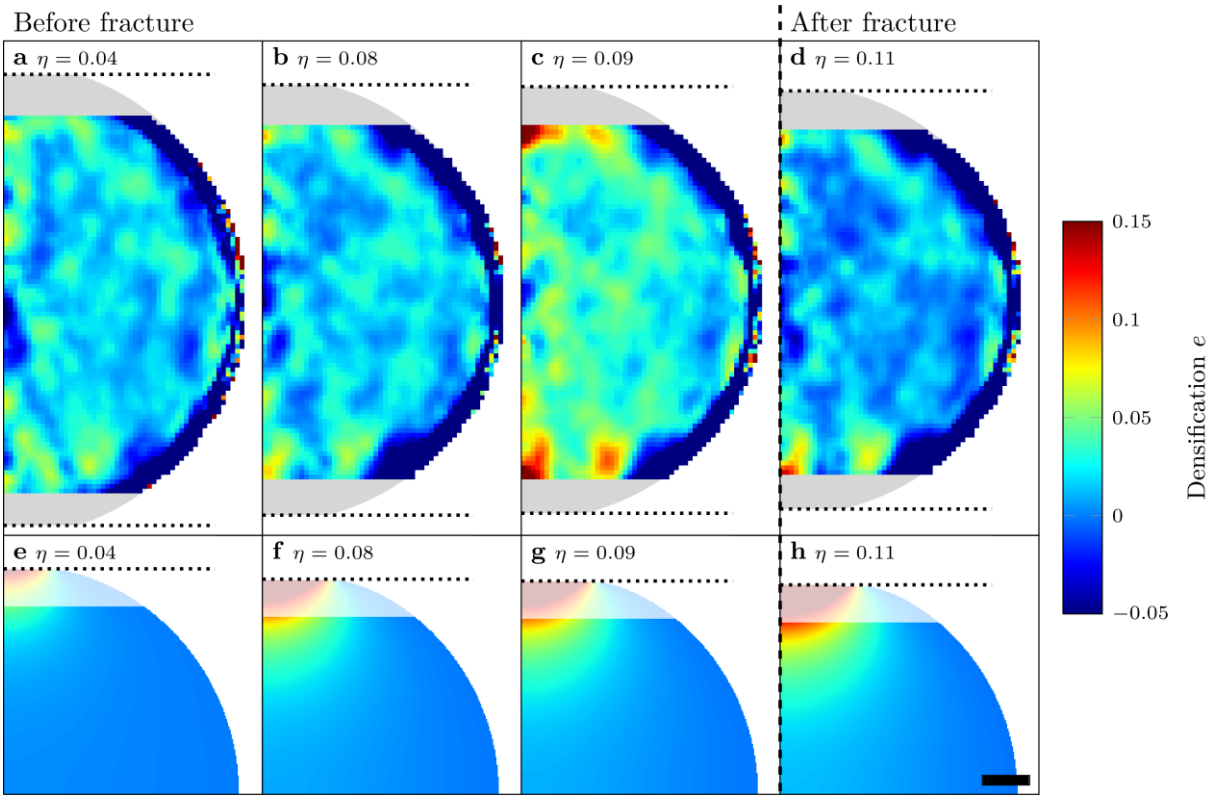

Figure 5. Measured (top row) and simulated (bottom row) rotationally averaged densification $\langle e(\mathbf{r})\rangle_\omega$ of the polymer core at increasing η for tomograms obtained before the appearance of fractures. The dotted lines indicate the stepwise changed positions of the sample holders, and the resulting η is indicated in each panel. Shading indicates regions shadowed by the sample holder. a-d) Quantitative measurements by ptychographic tomography. The compression causes increasing densification for a) through c) whereas the decrease in densification in d) is explained by the first signs of fracture appearing at this η, effectively giving strain relief. The negative densification observed along the surface of the bead is likely an artefact caused by the high electron density of the metal shell, impeding reliably measuring the electron density of the polymer. e-h) Predictions of densification by FEA. The magnitude and distribution of the calculated densification agree fairly well with the measured densification before fracture, i.e. for (a-c), while the stress relief by emerging fractures is not accounted for by the FEA model in h). Scalebar 1 μm.

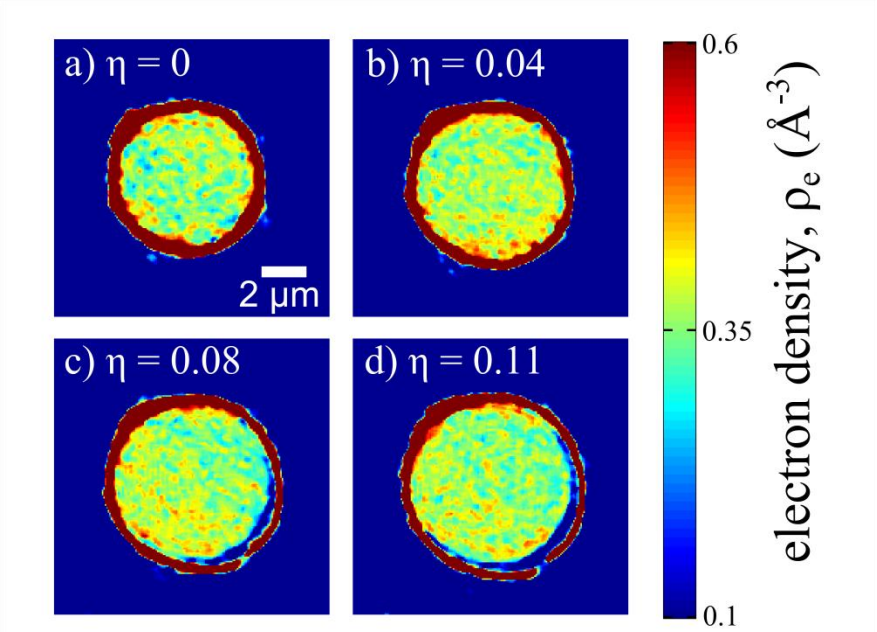

Figure 6. Tomographically reconstructed cross sections perpendicular to the compression axis, median filtered with a 7×7 square kernel to improve visualization. These cross sections were taken as close as possible to the upper contacting brass plate, which explains the apparently reduced composite diameter and the increased relative thickness of the metal coating. Efforts were made to ensure that similar regions are imaged in all four cases. Several of the topics discussed in the main text are clearly seen, including the rather uneven metallic coating, the delamination, and the fracture of the coating. The density distribution appears to be rather uniform for $\eta = 0$, to increase for $\eta = 0.04$ and 0.08, and to be somewhat relieved at $\eta = 0.11$, possibly related to the beginning fracture formation seen elsewhere in the polymer core. The color scale is chosen to emphasize features in the polymer core.

Table of contents entry

Title: Quantitative 3D X-ray Imaging of Densification, Delamination and Fracture in a Micro-Composite under Compression

*J. B. Fløystad, E. T. B. Skjønsfjell, M. Guizar-Sicairos, K. Høydalsvik, J. He, J. W. Andreasen, Z. Zhang, D. W. Breiby**

Keywords: X-ray microscopy; fracture mechanics; composites; tomography

Title: Quantitative 3D X-ray Imaging of Densification, Delamination and Fracture in a Micro-Composite under Compression

ToC figure:

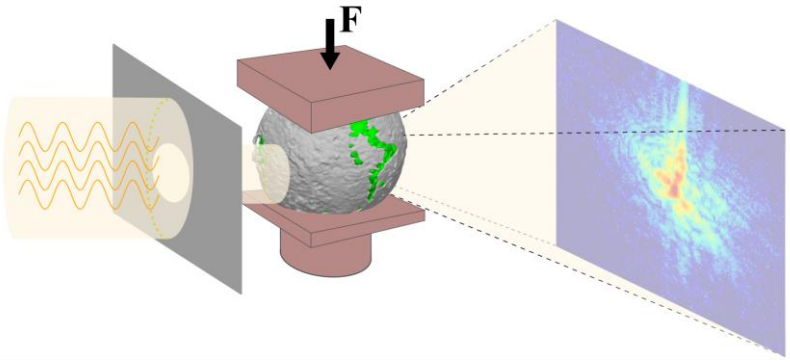

Ptychographic X-ray microscopy can be used for quantitatively studying the mechanical properties of microscale composites. Phase-contrast three-dimensional tomograms reveal with unprecedented detail the mechanical response, including delamination, densification and fracture, of a polymer-core / silver-shell micro-composite subjected *in situ* to a mechanical compression test.

(References):

[1] aS. M. Spearing, *Acta Materialia* **2000**, *48*, 179-196; bH. G. Craighead, *Science* **2000**, *290*, 1532-1535; cV. Kaajakari, *Practical MEMS*, Small Gear, Las Vegas, **2009**.

[2] K. L. Johnson, *Contact Mechanics*, Cambridge University Press, Cambridge, **1985**.

[3] M. van Hecke, *Journal of Physics-Condensed Matter* **2010**, *22*, 24.

[4] J. Y. He, Z. L. Zhang, H. Kristiansen, K. Redford, G. Fonnum, G. I. Modahl, *Express Polymer Letters* **2013**, *7*, 365-374.

[5] aP. Fratzl, R. Weinkamer, *Progress in Materials Science* **2007**, *52*, 1263-1334; bH. D. Espinosa, J. E. Rim, F. Barthelat, M. J. Buehler, *Progress in Materials Science* **2009**, *54*, 1059-1100; cA. M. Smith, S. M. Nie, *Accounts of Chemical Research* **2010**, *43*, 190-200.

[6] M. Chu, Y. K. Sun, U. Aghoram, S. E. Thompson, in *Annual Review of Materials Research, Vol. 39*, Annual Reviews, Palo Alto, **2009**, pp. 203-229.

[7] G. E. Sachs, W; Kuntze, W; Linicus, W, *Spanlose Formung der Metalle*, Springer, Berlin, **1931**.

[8] R. M. Schinagl, M. K. Ting, J. H. Price, R. L. Sah, *Ann. Biomed. Eng.* **1996**, *24*, 500-512.

[9] R. Bierwolf, M. Hohenstein, F. Phillipp, O. Brandt, G. E. Crook, K. Ploog, *Ultramicroscopy* **1993**, *49*, 273-285.

[10] Y. Tanaka, J. M. Yang, Y. F. Liu, Y. Kagawa, *Scripta Materialia* **2007**, *56*, 209-212.

[11] R. M. Simpson, J. Keegan, D. N. Firmin, *J. Magn. Reson. Imaging* **2013**, *37*, 576-599.

[12] K. Haldrup, S. F. Nielsen, J. A. Wert, *Experimental Mechanics* **2008**, *48*, 199-211.

[13] H. F. Poulsen, S. F. Nielsen, E. M. Lauridsen, S. Schmidt, R. M. Suter, U. Lienert, L. Margulies, T. Lorentzen, D. J. Jensen, *Journal of Applied Crystallography* **2001**, *34*, 751-756.

[14] H. F. Poulsen, J. A. Wert, J. Neuefeind, V. Honkimaki, M. Daymond, *Nature Materials* **2005**, *4*, 33-36.

[15] aM. C. Newton, S. J. Leake, R. Harder, I. K. Robinson, *Nature Materials* **2010**, *9*, 120-124; bP. Godard, G. Carbone, M. Allain, F. Mastropietro, G. Chen, L. Capello, A. Diaz, T. H. Metzger, J. Stangl, V. Chamard, *Nature Communications* **2011**, *2*.

[16] S. Sridharan, *Delamination behaviour of composites*, CRC Press, **2008**.

[17] P. J. Withers, M. Preuss, *Annual Review of Materials Research, Vol 42* **2012**, *42*, 81-103.

[18] P. A. M. O'Connell, G. B., *Yield and Crazing in Polymers*, Wiley, **2004**.

[19] H. S. Hosseini, A. L. Clouthier, P. K. Zysset, *Journal of biomechanical engineering* **2014**, *136*.

[20] J. Y. He, Z. L. Zhang, H. Kristiansen, *Journal of Applied Polymer Science* **2009**, *113*, 1398-1405.

[21] aJ. M. Rodenburg, A. C. Hurst, A. G. Cullis, B. R. Dobson, F. Pfeiffer, O. Bunk, C. David, K. Jefimovs, I. Johnson, *Physical Review Letters* **2007**, *98*, 034801; bP. Thibault, M. Dierolf, A. Menzel, O. Bunk, C. David, F. Pfeiffer, *Science* **2008**, *321*, 379-382.

[22] M. Holler, A. Diaz, M. Guizar-Sicairos, P. Karvinen, E. Farm, E. Harkonen, M. Ritala, A. Menzel, J. Raabe, O. Bunk, *Scientific Reports* **2014**, *4*.

[23] J. R. Fienup, *Appl. Opt.* **1982**, *21*, 2758-2769.

[24] aM. Dierolf, A. Menzel, P. Thibault, P. Schneider, C. M. Kewish, R. Wepf, O. Bunk, F. Pfeiffer, *Nature* **2010**, *467*, 436-439; bA. Diaz, P. Trtik, M. Guizar-Sicairos, A. Menzel, P. Thibault, O. Bunk, *Physical Review B* **2012**, *85*, 020104.

[25] aR. N. Wilke, M. Priebe, M. Bartels, K. Giewekemeyer, A. Diaz, P. Karvinen, T. Salditt, *Optics Express* **2012**, *20*, 19232-19254; bM. Esmaeili, J. B. Floystad, A. Diaz,

K. Hoydalsvik, M. Guizar-Sicairos, J. W. Andreasen, D. W. Breiby, *Macromolecules* **2013**, *46*, 434-439; cE. Lima, A. Diaz, M. Guizar-Sicairos, S. Gorelick, P. Pernot, T. Schleier, A. Menzel, *Journal of Microscopy* **2013**, *249*, 1-7.

[26] aB. Chen, M. Guizar-Sicairos, G. Xiong, L. Shemilt, A. Diaz, J. Nutter, N. Burdet, S. Huo, J. Mancuso, A. Monteith, F. Vergeer, A. Burgess, I. Robinson, *Scientific Reports* **2013**, *3*; bK. Hoydalsvik, J. B. Floystad, T. Zhao, M. Esmaeili, A. Diaz, J. W. Andreasen, R. H. Mathiesen, M. Ronning, D. W. Breiby, *Applied Physics Letters* **2014**, *104*.

[27] M. van Heel, M. Schatz, *J. Struct. Biol.* **2005**, *151*, 250-262.

[28] aF. Chowdhury, S. Na, D. Li, Y. C. Poh, T. S. Tanaka, F. Wang, N. Wang, *Nature Materials* **2010**, *9*, 82-88; bS. Mitragotri, J. Lahann, *Nature Materials* **2009**, *8*, 15-23; cK. J. Van Vliet, G. Bao, S. Suresh, *Acta Materialia* **2003**, *51*, 5881-5905.

[29] C. Sanchez, H. Arribart, M. M. G. Guille, *Nature Materials* **2005**, *4*, 277-288.

[30] D. Nam, J. Park, M. Gallagher-Jones, S. Kim, S. Kim, Y. Kohmura, H. Naitow, N. Kunishima, T. Yoshida, T. Ishikawa, C. Song, *Physical Review Letters* **2013**, *110*, 5.

[31] P. Kraft, A. Bergamaschi, C. Bronnimann, R. Dinapoli, E. F. Eikenberry, H. Graafsma, B. Henrich, I. Johnson, M. Kobas, A. Mozzanica, C. A. Schleputz, B. Schmitt, *IEEE Transactions on Nuclear Science* **2009**, *56*, 758-764.

[32] P. Thibault, M. Guizar-Sicairos, *New Journal of Physics* **2012**, *14*, 063004.

[33] M. Guizar-Sicairos, A. Diaz, M. Holler, M. S. Lucas, A. Menzel, R. A. Wepf, O. Bunk, *Opt. Express* **2011**, *19*, 21345-21357.

[34] A. C. S. Kak, M., *Principles of Computerized Tomographic Imaging*, IEEE Press, New York, **1988**.

[35] A. Chambolle, *Journal of Mathematical Imaging and Vision* **2004**, *20*, 89-97.

[36] Z. L. Zhang, H. Kristiansen, J. Liu, *Computational Materials Science* **2007**, *39*, 305-314.